

Structure and Excited-State Proton Transfer in the GFP S205A Mutant

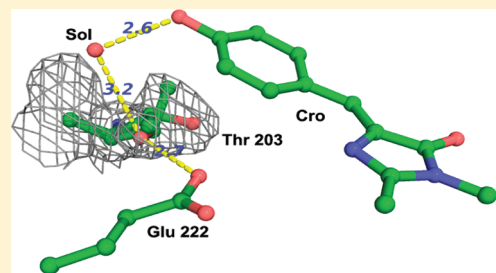
Yuval Erez,[†] Rinat Gepshtain,[†] Itay Presiado,[†] Kristina Trujillo,[‡] Karen Kallio,[‡] S. James Remington,[‡] and Dan Huppert^{*,†}

[†]Raymond and Beverly Sackler Faculty of Exact Sciences, School of Chemistry Tel Aviv University, Tel Aviv 69978, Israel

[‡]Institute of Molecular Biology and Department of Physics, University of Oregon 97403-1229, United States

Supporting Information

ABSTRACT: To further explore excited state proton transfer (ESPT) pathways within green fluorescent protein (GFP), mutagenesis, X-ray crystallography, and time-resolved and steady-state optical spectroscopy were employed to create and study the GFP mutant S205A. In wild type GFP (wt-GFP), the proton transfer pathway includes the hydroxyl group of the chromophore, a water molecule, Ser205, and Glu222. We found that the ESPT rate constant of S205A is smaller by a factor of 20 than that of wt-GFP and larger by a factor of 2 in comparison to the ESPT rate of S205V mutant which we previously characterized.¹ High resolution crystal structures reveal that in both S205A and S205V mutants, an alternative proton transfer pathway is formed that involves the chromophore hydroxyl, a bridging water molecule, Thr203 and Glu222. The slow PT rate is explained by the long (~3.2 Å and presumably weak) hydrogen bond between Thr203 and the water molecule, compared to the 2.7 Å normal hydrogen bond between the water molecule and Ser205 in wt-GFP. For data analysis of the experimental data from both GFP mutants, we used a two-rotamer kinetic model, assuming only one rotamer is capable of ESPT. Data analysis supports an agreement with the underlying assumption of this model.

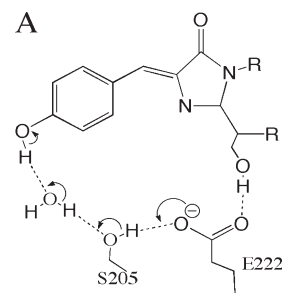


INTRODUCTION

The green fluorescent protein (GFP) is the prototypical example of a biological system in which excited state proton transfer (ESPT) plays a functional role in the mechanism of activity.^{2–6} GFP has two excitation bands, A (~390 nm) and B (~475 nm) corresponding to the neutral protonated and anionic forms of the chromophore, respectively. Steady state illumination of the A band results in green fluorescence, rather than blue emission as expected upon comparison with model compounds. Chattoraj et al.⁷ showed by ultrafast fluorescence upconversion spectroscopy that excitation at 388 nm results in instantaneous blue emission that decays to green with biphasic time constants of ~3 and ~12 ps. In the ESPT emission process, the excited state of the neutral chromophore first donates a proton to the carboxylate of Glu222, via a proton wire that involves a water molecule and the hydroxyl group of Ser205 as intermediate stations (see Scheme 1).^{8,9} Subsequently, the excited anion emits a green photon (termed I band emission). Data provided by Chattoraj et al.⁷ required that the emission of wild-type GFP be modeled by I and B states, where I* is the excited intermediate produced by the ESPT process. In contrast, emission from B* is caused by direct excitation of the B band, attributed to the chromophore anion in the ground state. In this manuscript, we do not address the emission process resulting from direct excitation of the B band, but for consistency the notation of Chattoraj et al. is retained.

Glu222 has been verified as the terminal proton acceptor by ultrafast vibrational spectroscopy.¹⁰ The proton transfer reaction is characterized by a deuterium isotope effect of 5–6,⁷ which is compared with multiple proton transfers as shown in Scheme 1.

Scheme 1. Schematic Diagram of the Proton Wire Found in Wild-Type GFP



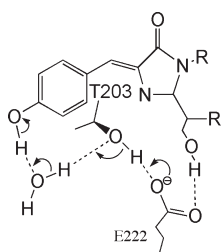
In a previous study we tested the role of Ser205 in the proposed wild-type ESPT pathway (Scheme 1) by mutating it to valine (S205V), which cannot support hydrogen-bonding and should therefore block the proton wire. However, time-resolved emission spectroscopy and a large deuterium kinetic isotope effect provided strong evidence that green fluorescence of S205V is nevertheless due to excited state proton transfer.¹ Proton transfer within the S205V mutant is observed to be 30-fold slower than wild-type. The crystal structure analysis of S205V indicated that structural and hydrogen bond rearrangements within the chromophore cavity led to an alternative ESPT pathway involving Thr203 instead of Ser205, with a long (~3.4 Å) hydrogen

Received: June 5, 2011

Revised: September 8, 2011

Published: September 08, 2011

Scheme 2. Schematic Diagram of Proton Wires Found in Both S205A and S205V Mutants of GFP



bond between Thr203 and the water molecule (see Scheme 2). The rate determining step in the overall proton transfer was attributed to this long hydrogen bond, which in turn supports the notion that proton transfer within GFP occurs via a concerted, rather than stepwise mechanism.¹⁰ Substitution of valine for Thr203 eliminated the alternative pathway, resulting in a novel blue fluorescent protein.¹

Here, we describe our spectroscopic and crystallographic studies of the mutant GFP/S205A, which was created to further explore the role of Ser205 in the proton wire. Alanine is less bulky than valine but is also incapable of supporting proton transfer. As seen in GFP/S205V, the new mutant is also green fluorescent. We show that an alternative proton wire is again formed by rearrangement within the chromophore cavity. Comparison of proton transfer rates and structures of the mutants provides insight regarding the geometric features that limit the rate of proton transfer.

EXPERIMENTAL SECTION

The S205A mutation was introduced into GFP, and protein was prepared as previously described for the mutant S205V.¹ Mutations were verified by sequencing the entire gene. Rectangular prism crystals of S205A were obtained in 2 days by hanging drop vapor diffusion. Crystallization setups consisted of 2 μ L drops containing one part protein solution ($A_{280} = 18.0$) in 50 mM Hepes, pH 7.9, 0.3 M NaCl and one part well solution. Crystals of S205A grew best in well solutions of 1.7 M malic acid, pH 7.0 with a 10% drop volume additive of 20% w/v benzamidine hydrochloride hydrate. X-ray diffraction data were collected at 100K to 1.79 Å resolution (limited by the crystalline order) using synchrotron radiation at beamline 5.0.1 at the Advanced Light Source, Berkeley.

The time-resolved emission of GFP S205A mutant in H₂O and D₂O solutions at low temperatures was obtained by the time-correlated single-photon-counting (TCSPC) technique. Excitation was provided by a cavity-dumped Ti:Sapphire femtosecond laser, (Mira, Coherent), which provides short (120 fs) pulses of variable repetition rates, operating at the second-harmonic-generation (SHG) frequency, over the spectral range of 380–400 nm with a repetition rate of 800 kHz. The TCSPC detection system is based on a Hamamatsu 3809U photomultiplier and Edinburgh Instruments TCC 900 computer module for TCSPC. The overall instrumental-response function (IRF) was about 35 ps full-width at half-maximum (fwhm). Measurements were taken over a spectral width of 10 nm. The excitation-pulse energy was reduced by neutral-density filters to about 10 pJ. The temperature of the sample was controlled by placing the sample in a

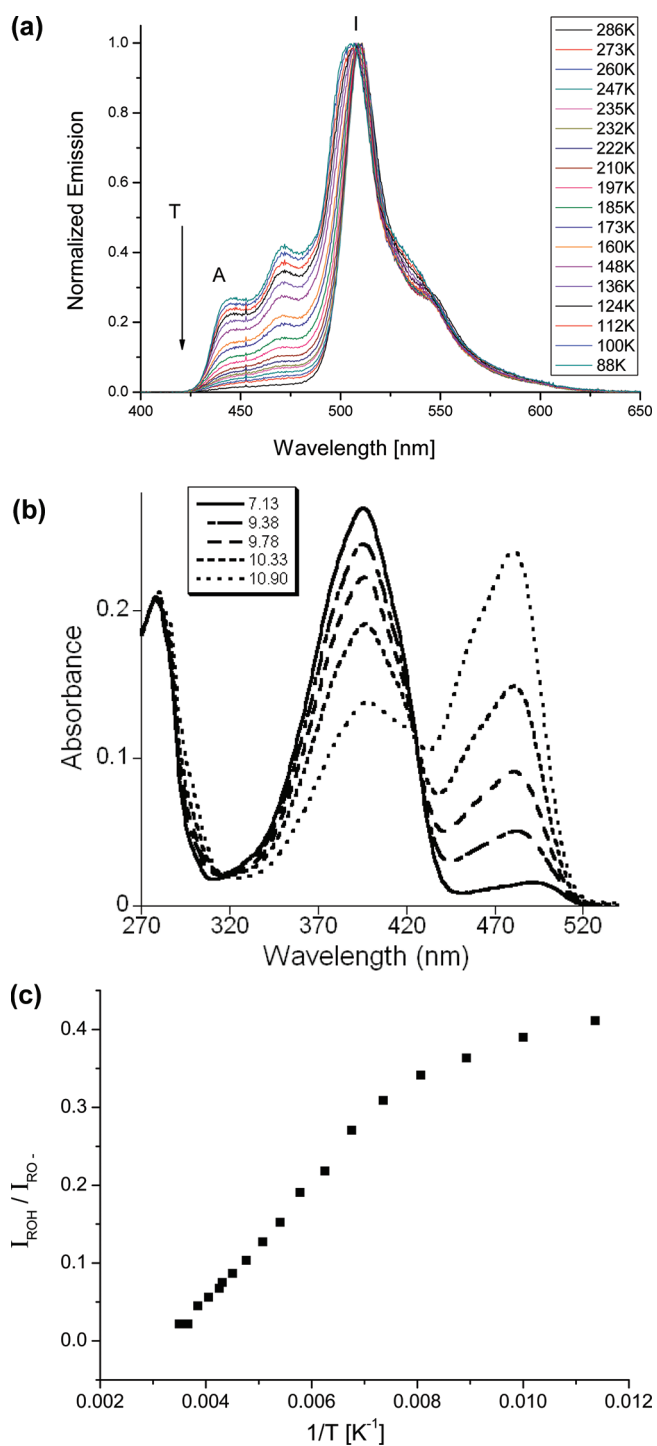


Figure 1. (a) Steady state emission spectra (excitation at 390 nm) of GFP S205A at pH \sim 7 as a function of temperature. (b) Absorbance spectra of GFP S205A as a function of pH. (c) Steady state amplitude ratio A/I for the protonated and deprotonated emission bands.

liquid-N₂ cryostat with a thermal stability of approximately ± 1.5 K.

The fluorescence up-conversion technique was employed in this study to measure the time-resolved emission of GFP S205A mutant in H₂O and D₂O solutions at room temperature. The laser used for the fluorescence up-conversion was the same laser as described above. The up-conversion system (FOG-100, CDP,

Russia) operated at 800 kHz. The samples were excited by pulses of ~ 8 mW on average at the SHG frequency. The time-response of the up-conversion system is evaluated by measuring the relatively strong Raman-Stokes line of water shifted by 3600 cm^{-1} . It was found that the fwhm of the signal is 280 fs. Samples were placed in a rotating optical cell to avoid degradation.

Steady-state measurements were conducted to measure the time-integrated emission spectrum of GFP S205A mutant at several temperatures. The laser used for the steady-state measurements was the same laser as described above. The sample was excited at 390 nm by the SHG of a cavity-dumped, mode-locked Ti:Sapphire laser operating at 800 kHz. The spectrum was collected by a miniature diode-array spectrometer CVI MS-240.

The proton transfer rate is calculated by fitting the signal of the protonated form measured at 450 nm by a biexponential fit. The fast decay-time component at room temperature has a lifetime of 150 ps which we attribute to the proton transfer process. The radiative lifetime of the protonated form is estimated to be $\tau_{\text{rad}} = 3\text{ ns}$ as the lifetime of the fluorescence of the deprotonated form emitting at $\sim 512\text{ nm}$.

RESULTS

Steady State and Time Resolved Spectroscopy. Figure 1a shows normalized steady-state fluorescence emission spectra of GFP S205A mutant at several temperatures in the range of 78–288 K, whereas Figure 1b shows the absorption spectrum at RT at several pH values. As is apparent from the absorbance spectrum, the chromophore is primarily in the protonated, neutral state at pH 7. However a small peak ($<5\%$ population) is observed at $\sim 495\text{ nm}$, indicative of the anionic chromophore. The percentage of the anionic form increases as the pH increases (Figure 1b), and the chromophore pK_a was estimated by fitting a standard titration curve to be >10 . Similar titration experiments show that the pK_a of the S205V chromophore is even higher. This is expected because the chromophore environment of S205V is more hydrophobic than in S205A.

Two overlapping emission bands are observed in Figure 1a. The A emission band is positioned in the blue part of the visible spectrum with a maximum around 470 nm. At low temperatures ($T \leq 182\text{ K}$) the A-band emission has a distinctive structure and comprises two major peaks, at 444 and 470 nm (see the Discussion). Similar substructure is also observed with the S205V mutant at low temperatures. The relative amplitude of the A-band increases with respect to the strong I-band amplitude (positioned at $\sim 515\text{ nm}$ at room temperature) as the temperature decreases. This was analyzed in more detail using a spectral fitting procedure to fit both the A- and I-bands. Each emission band is modeled by two vibrational bands, the shape of which is fit by a log-normal line-shape function with four adjustable parameters.

$$I(\nu) = h \begin{cases} \exp[-\ln(2)\{\ln(1 + \alpha)/\gamma\}^2] & \alpha > -1 \\ 0 & \alpha \leq -1 \end{cases} \quad (1)$$

$$\alpha \equiv 2\gamma(\nu - \nu_p)/\Delta \quad (2)$$

where ν_p , h , Δ , and γ are the peak position, amplitude, width and asymmetry, respectively. When $\gamma = 0$, the line-shape is Gaussian. Table S1 (in the SI) provides the fitting parameters of the log-normal fit function of steady-state emissions at 88 K and at

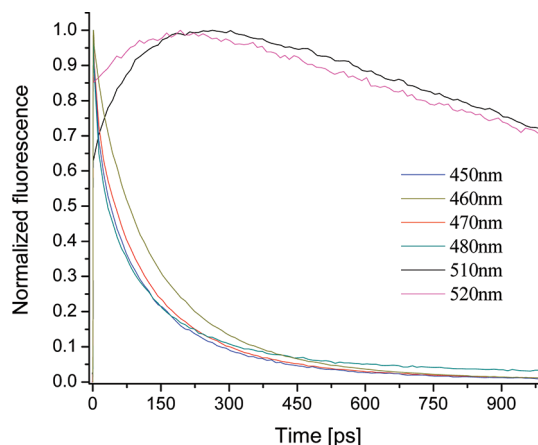


Figure 2. Time resolved up-conversion signal for GFP S205A measured at room temperature and at several discrete emission wavelengths, excitation at 390 nm.

222 K. The bandwidth of the deprotonated form is narrow, $\Delta \sim 650\text{ cm}^{-1}$ whereas for the protonated form it is wider by more than a factor of 2. This behavior is typical for the steady-state spectrum of wt-GFP and many other mutants including S205V. The sub-band peak position shift only slightly with temperature but their widths shrink as the temperature decreases. Figure 1c shows the relative amplitude of the A-band as a function of T^{-1} . The amplitude of the A-band increases roughly linearly with temperature until about 120 K where the slope sharply decreases, as may be observed in the plot.

Figure 2 shows time-resolved fluorescence up-conversion signals of GFP S205A mutant in aqueous buffered solution of pH ~ 7 at several wavelengths. The signals at short wavelengths ($\lambda \leq 480\text{ nm}$) appear extremely rapidly (within the instrument response time) and show a relatively slow decay with a time constant of about 150 ps. At longer wavelengths ($\lambda > 500\text{ nm}$) the signals exhibit an instrument-limited fast response, followed by a rise with a time constant of about 150 ps and a long decay of a few ns. The relative amplitude of the fast- and longer-rise components depends on the monitored wavelength. In general, the fluorescence up-conversion signals indicate simple excited kinetics, portraying an initial species (A-form) that emits at a short wavelength and transforms into a new, longer wavelength emitting species (I state). At longer wavelengths ($\lambda > 480\text{ nm}$) the two emission bands, that of the A-form and that of the I-form, overlap and thus the signals measured even at longer wavelengths ($\lambda > 520\text{ nm}$) exhibit short and long rising components. The short component with relative amplitude of about 0.6 is attributed to the emission of the protonated form (the A-form or ROH) whereas the long rise component is attributed to the I-form (the deprotonated form, the RO⁻) with its emission band peak positioned at 515 nm.

Figure 3a compares on a semilogarithmic scale the fluorescence up-conversion signals of the A-band of wt-GFP and the two mutants S205A and S205V, measured at 460 nm. As seen in the figure, the wt-GFP signal decay is fast with $\langle\tau\rangle = 8\text{ ps}$ whereas the decay-time of the two mutants is much longer. Figure 3b compares on a semilogarithmic scale, the fluorescence up-conversion signals of the I-band of the same three proteins as in Figure 3a, measured at 510 nm. The signal rise of the wt-GFP is rather short, whereas the signal rise of the two Ser205 mutants is

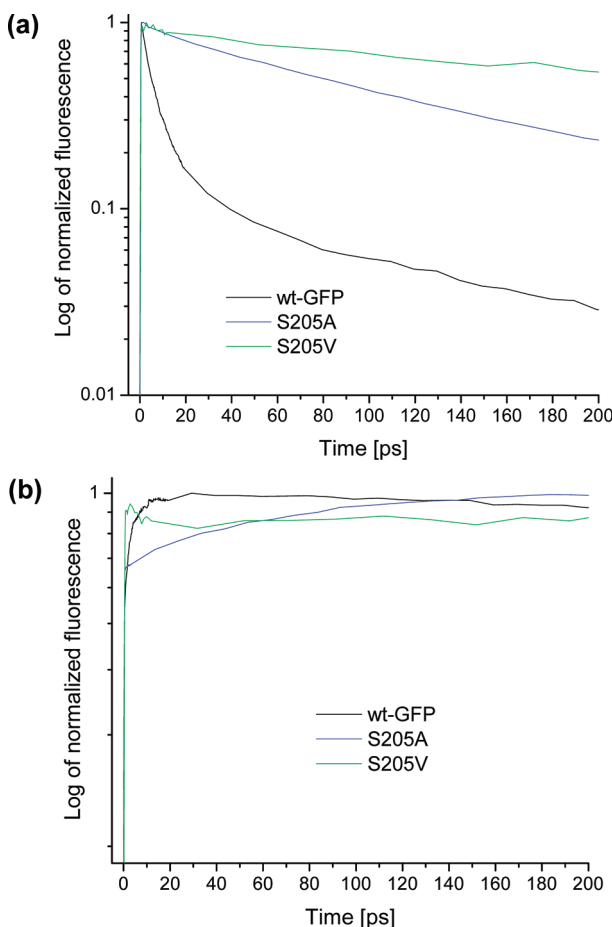


Figure 3. Time resolved up-conversion signal of wt-GFP, S205A and S205V in H_2O , excited at 390 nm and detected at (a) 460 and (b) 510 nm.

much longer. We attribute the fast decay (at 460 nm) and rise (at 510 nm) of the wt-GFP emission to the efficient intermolecular excited-state proton transfer (ESPT) process of the chromophore.

Figure 4a shows the time-resolved emission of the A (ROH) band of the S205A mutant in aqueous buffered solution at pH ~ 7 , measured at 460 nm in several temperatures over the temperature range of 78–288 K. The sample was excited at 390 nm with the same laser used in the fluorescence up-conversion measurements shown in Figure 2.

As seen in the figure, the lower the temperature the longer the average decay-time of the emission signal. The signal decay-time at room temperature conforms to the value derived from the fluorescence up-conversion signal. We attribute the large temperature dependence of the A-band decay rate to the large temperature dependence of the proton transfer rate from the chromophore to the E222 glutamate. For wt-GFP the temperature dependence of the proton transfer rate is much smaller, whereas for S205V it is comparable to that found in the current study.

Figure 4b shows the TCSPC signal of the same sample as shown in Figure 4a, measured at 515 nm, near the emission peak of the I (RO^-) band. The signal at short times increases as time progresses and the time-resolved emission reaches a maximum at around 0.5 ns. At longer times the signal decays nearly exponentially with a decay-time of about 3 ns. The signal rise-time shortens with increase in temperature. Due to the finite radiative decay-time

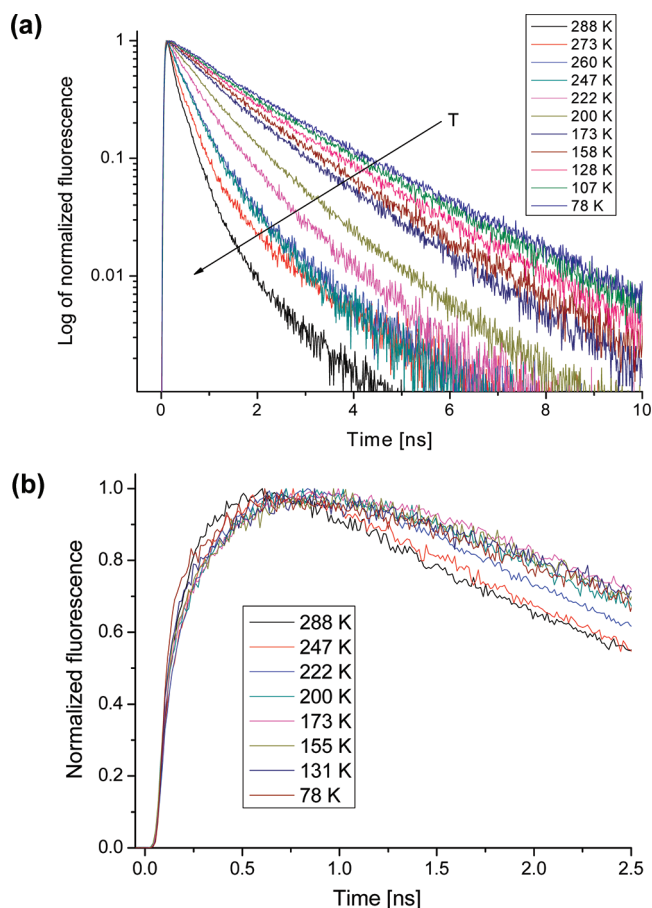


Figure 4. Time resolved emission measured by time-correlated single photon counting technique of S205A/ H_2O excited at 400 nm. Detected at (a) 460 and (b) 510 nm.

(3 ns), the overall time profile of the I-band TCSPC signal is less sensitive to temperature than the complementary signal decay of the A-band, shown in Figure 4a. Thus, in general the protonated form A-band decay profile provides more information with a much better S/N ratio.

Kinetic Isotope Effects. Figure 5 shows the normalized steady-state emission of S205A in D_2O at several temperatures in the range of 88–295 K. At high temperatures, the relative emission intensity of the A band (peak ~ 460 nm) is much lower than that of the I band (peak ~ 512 nm). In general, the A emission band relative intensity increases as the temperature decreases. The temperature dependence of the emission intensity ratio $I_{\text{ROH}}/I_{\text{RO}^-}$ is not constant and can be roughly divided to two regimes, above $T > 250$ K where it is large and below 250 K where it is rather small.

Figure 6a shows the TCSPC signals of the GFP S205A mutant A-form emission band in D_2O , measured at several temperatures over the range of 79–345 K. The decay rates of the samples at $T \leq 258$ K show rather small temperature dependence, the average decay-time at 88 K being $\langle \tau \rangle \tau \approx 2$ ns.

Figure 6b shows the time-resolved emission of GFP S205A mutant in D_2O , measured at several wavelengths in the spectral range of 430–520 nm by TCSPC technique at a single low temperature of ~ 80 K. As seen in the figure the signals grouped into two subsets, in the blue and green parts of the spectrum. As in

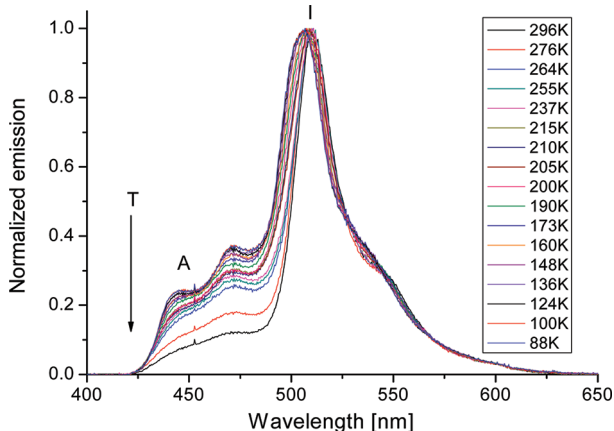


Figure 5. Steady state emission of S205A in D_2O , excited at 390 nm.

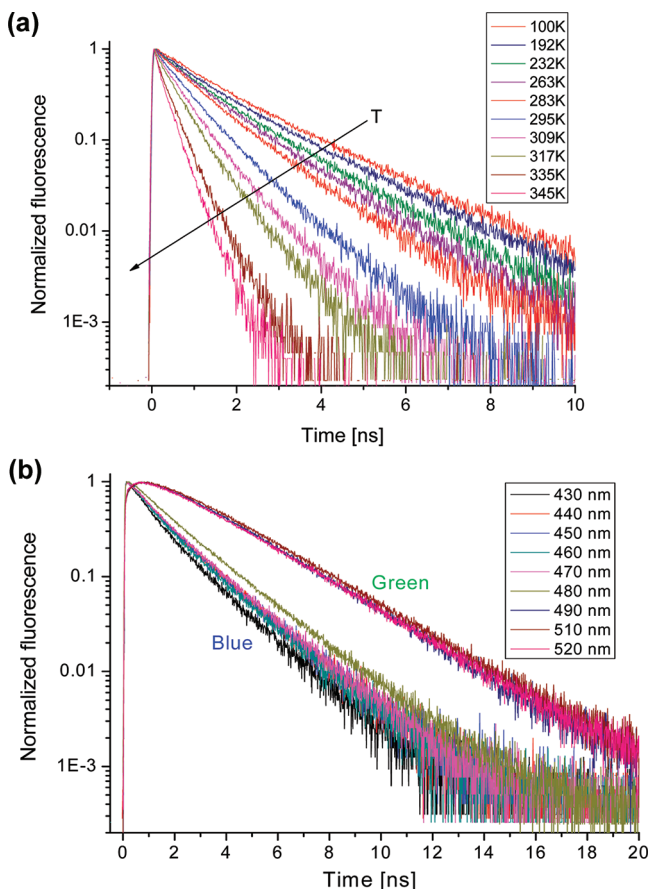


Figure 6. (a) Time resolved emission of S205A in H_2O measured at several temperatures; detected at 460 nm (b) Time resolved emission of S205A in D_2O measured at several wavelengths; $T = 79$ K.

H_2O , the D_2O signals are consistent with a simple photoreaction in which an initial single reactant (the A-band emitter) forms a single product (the green fluorescence I-band emitter). The decay-time of the A-band is about 2 ns, almost independent of the measured wavelength. The TCSPC signals of the I-band monitored at long wavelengths ($\lambda \geq 490$ nm) show a distinct rise-time with a complementary time-component of ~ 2 ns, similar to the decay-time of the A-band. The TCSPC signals shown in figure 6b

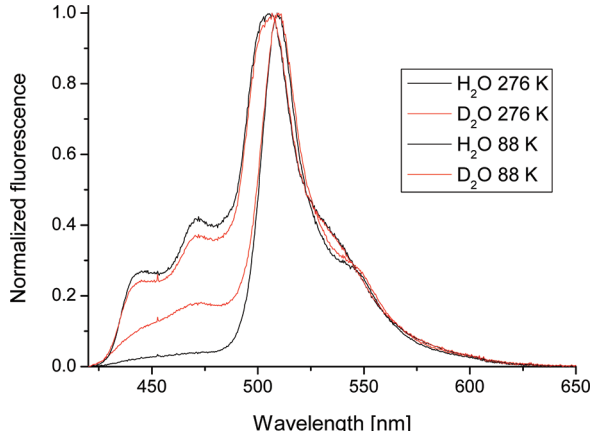


Figure 7. Comparison of the steady state emission of S205A in H_2O and D_2O at two temperatures 88 and 276 K.

indicate that deuteron-transfer reaction indeed occurs in D_2O solvent at 79 K, the lowest temperature measured in the study.

Figure 7 shows a comparison of the normalized steady-state emission of H_2O and D_2O samples at low and high temperatures. The A-band signal intensities of the D_2O samples are much larger than those of the H_2O samples at high temperatures. The ratio between the protonated and deprotonated steady-state emission signals (A- and I-bands of wt-GFP and each mutant) is strongly related to the proton-transfer rate. The larger signal of the D_2O sample A-band provides a good estimate for the large proton-transfer kinetic isotope effect (KIE) in the GFP S205A mutant, $\text{KIE} \sim 5$ at 290 K. The interesting point in the comparison between H_2O and D_2O samples is that in the low temperature region, the KIE decreases.

Figure 8 shows a comparison of the GFP S205A mutant A-band TCSPC signals in H_2O and D_2O at several temperatures. At high temperatures the decay-time of the A-band in D_2O samples is much longer than in H_2O water and thus the KIE of the proton/deuteron transfer reaction is large, $\text{KIE} \sim 5.5$. At low temperatures the decay rate of the A-band emission is about the same for H_2O and D_2O samples and thus we estimate that the KIE drops to close to 1. A similar phenomenon is also found in the steady-state emission comparison shown in Figure 7.

Crystallographic Results. The crystals of GFP/S205A have space group R32, with one molecule in the asymmetric unit and permitted diffraction data to be collected at cryogenic temperature (100 K) to 1.79 Å resolution. The crystal structure was solved by molecular replacement using wild type GFP as the starting model and the S205A model was refined at 1.82 Å resolution. The atomic model has good geometry and the crystallographic refinement statistics are satisfactory. Data collection and model refinement statistics are provided in Table S2.

Overall, the structure of S205A GFP is nearly identical to that of wild-type GFP. Two bound benzimidine molecules were located in a small cavity near an intermolecular interface, consistent with the requirement for this compound in the crystallization buffer. An internal rearrangement is observed close to the site of mutation, evidently caused by the lack a hydrogen bond donor or acceptor at the 205 position. As a result, a different hydrogen-bonded network is formed, involving the chromophore hydroxyl, a bridging water molecule, Thr203 and Glu222 (Scheme 2). We propose that this network is responsible for ESPT, as observed in the S205V mutation.

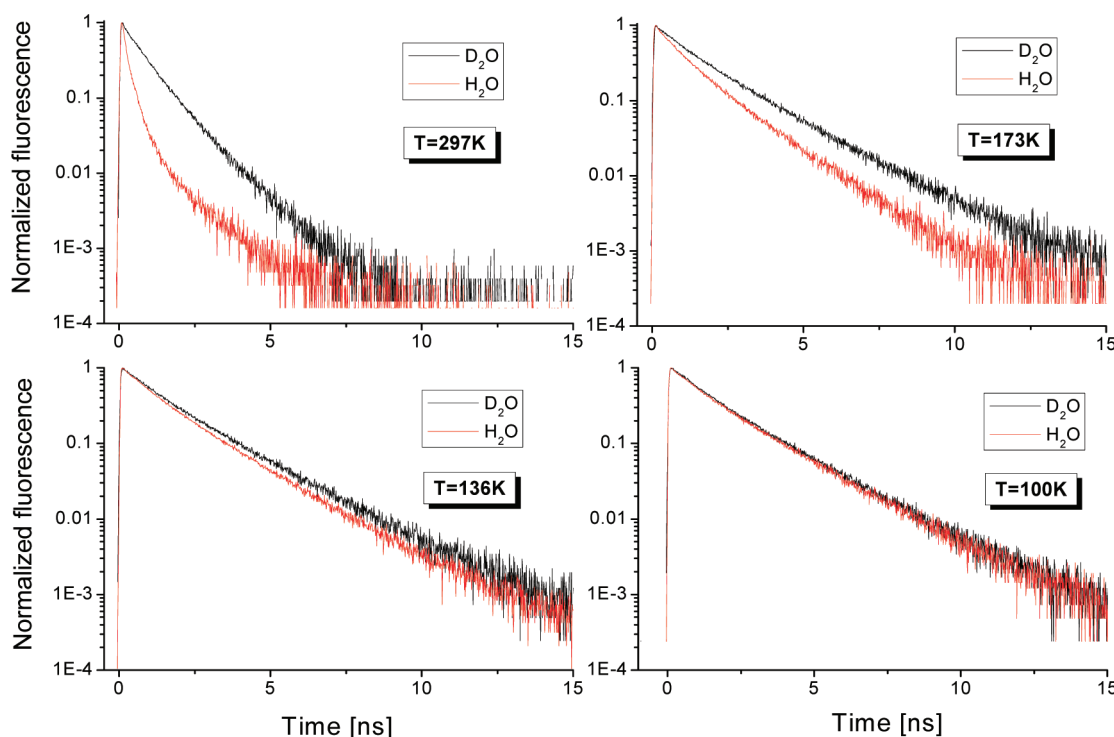


Figure 8. Comparison of time-resolved emission at four temperatures. The sample was excited at 400 nm and emission was detected at 460 nm.

A complication with this interpretation is that the electron density map at 100 K clearly reveals Thr203 to occupy two rotameric configurations, distinguished by χ_1 angles of $\sim 170^\circ$ and $\sim 305^\circ$ (Figure 9). Analysis of the density map using the program Ringer¹¹ confirmed this finding. Accordingly, the Thr 203 side chain was modeled with two conformers at 50% occupancy each and after crystallographic refinement the thermal (B) factors for each rotamer converged to similar values ($\sim 20 \text{ \AA}^2$), supporting the assignment of equal occupancies. In the $\chi_1 \sim 170^\circ$ configuration, Thr 203 O γ participates in the putative proton wire shown in Scheme 2. The O γ is involved in a long ($\sim 3.2 \text{ \AA}$ and therefore presumably weak) hydrogen bond with a solvent molecule (designated 19 in the structure), and a normal hydrogen bond of length $\sim 2.7 \text{ \AA}$ with the carboxylate group of Glu 222. In the alternative rotameric configuration ($\chi_1 \sim 305^\circ$), Thr 203 O γ does not appear to make any hydrogen bonds. The fact that the two conformations are in approximately equal occupancy suggests that the two side chain environments are energetically very similar, and that the O γ -solvent hydrogen bond is either weak or similar in strength to the non-bonded contacts made in the alternative configuration.

The observed rotameric configurations of Thr 203 ($\chi_1 = \sim 170^\circ$ and $\sim 305^\circ$) are partially eclipsed, and correspond approximately to the two least frequently observed configurations of Thr in proteins ($\chi_1 = 62^\circ, 49\%$; $\chi_1 = 305^\circ, 43\%$; $\chi_1 = 185^\circ, 7\%$; see the compilation by Lovell et al.¹²). This indicates that the rotational freedom of the Thr 203 side chain is severely restricted and consequently, the rate of interconversion of the two conformations is probably quite slow, on the order of milliseconds to seconds. Hence, one must consider that in solution there are two populations of GFP molecules, one population with a proton wire and the other without.

The two configurations observed for Thr 203 provide a possible interpretation for the two resolved peaks observed in

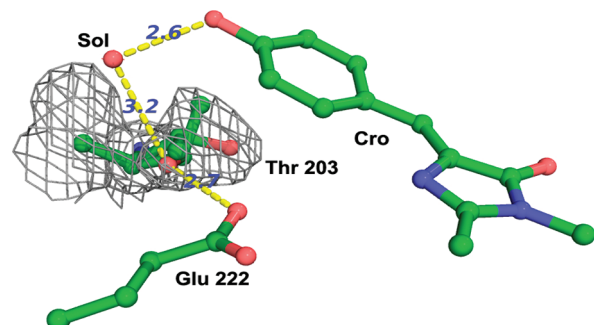


Figure 9. Ball and stick representation of the refined crystallographic model of GFP S205A, showing details of the proton wire. Hydrogen bonds are shown as yellow dashed lines and have the indicated lengths in \AA . The wire cage around Thr203 shows the 2Fo-Fc electron density calculated after omitting the side chain of Thr203, contoured at 1.0 standard deviations. Both observed rotameric states of the Thr203 side chain are shown.

the blue, high energy portion of the S205A emission spectrum. The time-resolved emission decay profiles in the spectral region of 440–480 nm are almost identical. Therefore, there is no support for the hypothesis that the two bands seen in the steady-state emission arise from two rotamers that only one of which can transfer a proton to glutamate E222. As evidenced by the spectroscopic studies (especially Figure 1b), the chromophore of GFP S205A is normally protonated. The OH group participates in two hydrogen bonds, one to His 148 N δ 1 and the other to water 19 (Figure 10). Thus, its hydrogen bonding potential is saturated. However, the strength of those hydrogen bonds will depend on the second hydration shell of the chromophore OH, which includes Thr 203 O γ .

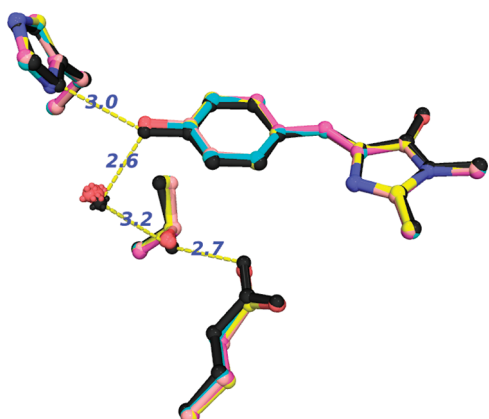


Figure 10. Ball and stick representation of the refined crystallographic models for GFP S205V and GFP S205A, showing hydrogen bonds and other details of the proton wires. The water molecule that participates in the proton relay is shown as red crosses (S205V, four molecules in the asymmetric unit) or as a black cross (S205A). The individual copies of each example in the asymmetric units of the crystals were superimposed by an all-atom least-squares procedure prior to producing the figure. The residues comprising the S205A proton wire are drawn with black carbon–carbon bonds. Of special note is that the black cross (water in S205A) is displaced relative to the red crosses, resulting in a slightly shorter hydrogen bond to Thr 203.

Furthermore, the presence of the two Thr 203 rotamers in the mutant S205A, caused us to re-examine the electron density map and model for the mutant S205V. In this case there are four independent protomers in the asymmetric unit of the crystal, which give four independent views. Prominent features in the Fo-Fc difference electron density map indicated the same two rotameric configurations for Thr 203, so the model for S205V was reinterpreted in the light of the new data. The same two rotameric configurations of Thr 203 are evident in all four subunits and in each case are consistent with the interpretation for S205A. After reinterpretation of the model and subsequent crystallographic refinement, the geometry of the Thr configuration providing the proton wire remains as originally reported by Shu et al.¹ Averaged over the four subunits in the asymmetric unit, the water-Thr 203 O γ hydrogen bond distance is 3.30 ± 0.16 Å, which is again unusually long and probably very weak.

An important feature of the new ESPT pathway, now identified in both GFP S205V and S205A, distinguishes them from that found in wt-GFP. The average distance from the bridging water molecule to Thr203 O γ is ~ 3.2 Å for S205A mutant and ~ 3.3 Å in the S205V mutant, suggesting that in both cases, the hydrogen bond between the water molecule and the hydroxyl is weak. It seems likely that the large gap between the bridging water molecule and Thr203 OG1 results in infrequent proton transfer. A caveat to this argument is that the differences between the water-Thr 203 O γ distances in the two structures are statistically at the level of the coordinate error, estimated for these structures to be ~ 0.1 Å rms by using Cruickshank's formula.¹³ For comparison, the distance between the bridging water and the hydroxyl of Ser 205 in wt-GFP is normal, ~ 2.7 Å.

Keeping in mind that there are four copies of the protein in the S205V crystal and one in the S205A crystal, an overlay of the five models is shown in Figure 10. The individual copies of the S205V proton wire, including the water molecule position (red crosses) cluster tightly, whereas the water molecule in S205A (black cross) appears in the figure to be closer to the Thr position.

■ DISCUSSION

A summary of the steady-state and the time-resolved optical studies is as follows:

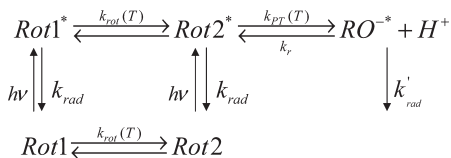
1. The chromophore of GFP-S205A is primarily in the protonated state at neutral pH and room temperature, yet gives rise to predominantly green fluorescence emission. This is attributed to ESPT between the chromophore OH and Glu 222.
2. At room temperature, the proton transfer rate of the GFP S205A mutant in water is relatively slow, $\tau_{\text{PT}} = 155$ ps, $k_{\text{PT}} = 6.5 \times 10^9$ s $^{-1}$ compared to the wt-GFP $k_{\text{PT}} = 1.25 \times 10^{11}$ s $^{-1}$, i.e., about 20 times slower. By comparison, the mutant GFP S205V shows a yet slower rate of proton transfer, 4.1×10^9 s $^{-1}$ at room temperature, or about 30 times slower than wild type.
3. The temperature dependence of the proton transfer rate does not obey a simple Arrhenius plot with a constant slope. The slope of an Arrhenius plot decreases as the temperature decreases. The overall plot shows a concave shape with a break at about 220 K, the so-called protein “glass transition”. For the approximately linear portion of the Arrhenius plot above this temperature, the slope corresponds to an activation barrier of about 15 kJ/mol. At temperatures below 175 K the slope of the Arrhenius plot is rather small, less than 1 kJ/mol.
4. At low temperatures $T < 175$ K, the proton transfer rate reaches an asymptotic value of $\sim 3 \times 10^8$ s $^{-1}$, reduced by a factor of 15 from the value at room temperature.
5. The time-integrated spectra and the time-resolved emission indicate that the proton transfer process at room temperature exhibits a large kinetic isotope effect (KIE) in the GFP S205A mutant. The KIE is about that of wt-GFP, KIE ~ 5 .
6. The temperature dependence of k_{PT} of GFP S205A mutant in D₂O is larger than in H₂O. At $T \approx 235$ K, k_{PT} in D₂O at low temperatures is constant and fairly large, $k_{\text{PT}} = 3 \times 10^8$ s $^{-1}$. Thus the effective KIE strongly decreases at low temperatures and approaches the value of ~ 1 .

From the crystal structure similarity one would expect then that the proton transfer rate and its temperature dependence will also have similar values, as indeed they do. The proton transfer rate constants for S205A and S205V at room temperature are 6.6×10^9 and 3.3×10^9 s $^{-1}$ respectively. The wt-GFP proton-wire is much more suitable for proton shuttle and thus the average PT rate constant is 1.25×10^{11} s $^{-1}$. The kinetic isotope effect (KIE) at room temperature is ~ 5 for both mutants and also for wt-GFP. The KIE value for a photoacid in homogeneous environment of bulk water or alcohol is smaller, KIE ~ 3 . In both mutants the effective KIE decreases as a function of temperature and approaches the value of 1 at 175 K and below, whereas in wt-GFP, the KIE maintains its high value at all the temperature studied, i.e., $T \geq 80$ K.

The spectroscopic behavior shows that the alternative ESPT pathway through the Thr203 residue is very similar for these two mutants. In S205A, the long bond between the hydroxyl oxygen of the bridging water and Thr 203 appears shorter, 3.2 Å compared to 3.3 Å in S205V, consistent with the larger PT rate in S205A.

If the rate of proton transfer from the chromophore to the bridging water molecule is limited by proton transfer from the bridging water to Thr203, these data suggest that the overall process of proton transfer within S205A and S205V mutants to

Scheme 3



the ultimate acceptor, Glu 222, is concerted. Alternatively, Fang et al.¹⁴ have recently described ultrafast time-resolved Raman spectroscopy of wt-GFP and have suggested that concerted motions of the chromophore, with a period of about 280 fs, are responsible for initiating the proton transfer process. The dynamics of the GFP-chromophore system could well be different in the mutants S205A and S205V, and if those dynamics form the basis for the rate-limiting process, then one would not expect to explain PT rates based on subtle geometric differences between the crystal structures.

Modeling the Temperature Dependence of Proton Transfer. The X-ray crystallographic analysis shows that the Thr203 residue in both the S205A and S205V mutants has two rotamers, which we designate as Rot1 and Rot2 in scheme 3. Rot1 cannot transfer a proton at all temperatures since it does not form a hydrogen bond with the water molecule W19, whereas Rot2 can transfer a proton to the glutamate at a moderate rate since the hydrogen bond length between Thr203 and the W19 is rather long, 3.2 and 3.3 Å for S205A and S205V, respectively, compared to about 2.7 Å for the rest of the proton wire. Scheme 3 provides the kinetic scheme that includes excitation of the GFP chromophore in both rotamers of the Thr203 by a short laser pulse, the excited state emission, rotamer interconversions and proton transfer from the chromophore of the glutamate via Thr203 residue. At room temperature, the two different time-resolved techniques used in this study both show a nearly exponential decay of ROH emission, with a major fast component of time constant $\tau = 150$ ps at room temperature, followed by a slow component of about 1 ns with amplitude ~ 0.05 . This result implies that if two rotamers exist and their initial population is half then the rotation rate is larger than the PT rate, i.e., $k_{rot} > k_{PT}$. If we assume the opposite case for which the excited state proton transfer rate constant $k_{PT} > k_{rot}$, where k_{rot} is the rotation rate constant, one would expect biexponential decay of the ROH, the protonated form of the chromophore, provided that the emission band position and intensity is independent of the rotamers Rot1 and Rot2. For equally sized populations of both rotamers at the ground state the amplitude of the two time components of the ROH* emission would be equal (0.5).

NMR data suggest that rotamer interconversion rates for Thr can range from nanoseconds to seconds.¹⁵ Because in our example the two rotamers occupied by Thr203 are the two least favored and neither conforms to the optimal staggered configuration, the environment is probably very restricted and the interconversion rate is much longer than nanoseconds (milliseconds to seconds), even at RT. Therefore in our two rotamer model we assume that interconversion between the two rotamers does not occur after excitation, but only in the ground-state, where equilibrium between the two rotamers can be reached at sufficiently long times. When Rot2 is excited by the short laser pulse (see Scheme 3), PT to the glutamate may occur.

Another parameter that one needs to take into account and may affect both the fluorescence quantum yield and the time-resolved

Table 1. Fitting Parameters for the Time-Resolved Exponential Analysis of the S205A Mutant in Water^a

temperature (K)	τ_1	b_1	τ_2	b_2	χ^2
78	1.00	0.46	2.10	0.54	0.680
131	1.03	0.58	2.06	0.42	0.100
155	0.79	0.52	1.72	0.48	0.672
173	0.62	0.63	1.44	0.37	0.578
222	0.42	0.79	1.18	0.21	0.503
247	0.24	0.92	1.32	0.08	0.599
288	0.19	0.94	0.97	0.06	0.559

^a $y = \sum_{i=1}^2 b_i e^{-t/\tau_i}$.

emission decay signal is the nonradiative rate of the chromophore. HBDI, the synthetic chromophore analog exhibits an extremely short emission decay time which is explained by a large nonradiative rate due to fast angle twisting between the two ring systems. In general the nonradiative rate depends on the rotation angle between the two ring subsystems of the chromophore. We expect that the nonradiative rate be temperature independent below the protein glass transition around 220 K.

An experimental result that should be taken into account is the isotope effect caused by deuteration of the sample buffer, which may affect both the time-resolved and the steady state emission results. The steady-state and the time-resolved emission of S205A in D₂O at room temperature show that the decay rate of the chromophore ROH emission band is distinctively slower than in H₂O and the temperature dependence of k_{PT} at temperatures larger than 220 K is much larger in D₂O. The activation energies of k_{PT} are 15 and 30 kJ/mol for H₂O and D₂O samples, respectively. For wt-GFP the activation energies of PT are much lower and the difference in the activation energy between H₂O and D₂O is rather small.^{16,17}

Two Rotamers Model: the Biexponential Analysis. Assumptions and experimental facts

1. Thr203 has two rotamers.
2. The interconversion time between the rotamers is much longer than the excited-state lifetime, and therefore, the PT process can only happen for Rot2 that is excited from its ground-state. The second rotamer's excitation (Rot1) does not lead to its interconversion to Rot2 and to the subsequent PT and formation of ROH*.
3. Only one of the rotamers can transfer a proton from H₂O through Thr203 to the final proton acceptor.

The biexponential decay analysis of the time-resolved emission of the ROH* signal provides three parameters: the population ratio of the two rotamers and the two decay times, τ_1 and τ_2 . Tables 1 and 2 provide the parameters of a biexponential kinetic analysis for the S205A mutant in H₂O and D₂O samples respectively. Tables s3 and s4 provide the data analysis parameters of a biexponential fit of the time-resolved emission of the S205V mutant. τ_1 provides information on the PT rate, and τ_2 is the decay time of the ROH* form of the chromophore of Rot1, the PT-incapable rotamer. Therefore, τ_2 is determined by the radiative and nonradiative processes. If we assume that the radiative and nonradiative rates of both rotamers are the same, then we can write

$$\frac{1}{\tau_2} = k_r + k_{nr} \quad (3)$$

where k_r and k_{nr} are the radiative and nonradiative decay rate constants of the electronically excited ROH* form of the

Table 2. Fitting Parameters for the Time-Resolved Exponential Analysis of the S205A Mutant in Deuterated Water^a

temperature (K)	τ_1	b_1	τ_2	b_2	χ^2
100	1.10	0.49	2.19	0.51	0.670
192	0.96	0.48	2.03	0.52	0.731
263	0.80	0.45	1.57	0.55	0.589
295	0.61	0.63	1.10	0.37	0.499
317	0.42	0.68	0.77	0.32	0.328
335	0.25	0.55	0.46	0.45	0.290
345	0.13	0.37	0.34	0.63	0.297

$$^a y = \sum_{i=1}^2 b_i e^{-t/\tau_i}$$

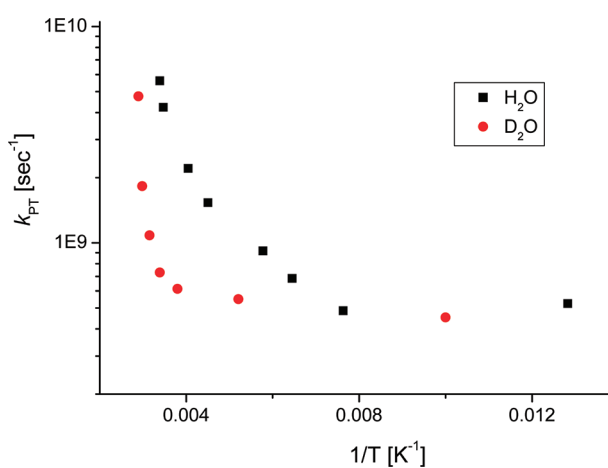


Figure 11. Arrhenius plot of $\ln k_{PT}$ versus $1/T$ for the two rotamers analysis of the time-resolved emission signals for both H_2O and D_2O samples.

chromophore respectively. From the tables it is seen that at sufficiently low temperatures τ_2 for both H_2O and D_2O is about the same. Thus, as expected k_{nr} is about the same for both H_2O and D_2O . τ_1 is shorter than τ_2 since Rot2 undergoes a PT. This leads to

$$\frac{1}{\tau_1} = k_{PT} + \frac{1}{\tau_2} \quad (4)$$

The PT rate constant k_{PT} can now be deduced from the two lifetimes of the biexponential decay of the ROH^* emission

$$k_{PT} = \frac{1}{\tau_1} - \frac{1}{\tau_2} \quad (5)$$

Figure 11 and figure s2 show an Arrhenius plot of $\log k_{PT}$ versus of $1/T$ for both S205A and S205V mutants in H_2O and D_2O data. k_{PT} was calculated using eq 5. The temperature-dependence of the PT rate is not as straightforward as expected from a simple activated process. At high temperatures the slope of the Arrhenius plot is precipitous, but as the temperature decreases the slope becomes more and more moderate, so that the overall shape of the plot is concave. The activation energy of the PT/DT process at high temperatures is ~ 15 and ~ 30 kJ/mol in H_2O and D_2O , respectively. At $T < 220$ K in D_2O or at $T < 150$ K in H_2O , k_{PT} becomes temperature independent, and its asymptotic value is $4 \times 10^8 \text{ s}^{-1}$. Similar temperature-dependence and absolute values of k_{PT} could be derived from a simpler analysis of the time-resolved

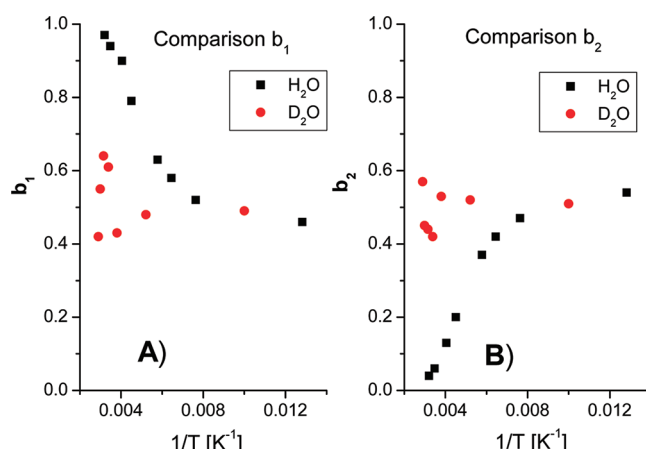


Figure 12. Amplitude of both the fast and slow time components as a function of $1/T$: (A) the fast component and (B) the slow component.

emission data. Data analysis of both S205A and S205V yields similar results. The major difference between the kinetic parameters of the two mutants is that the S205A mutant has a larger k_{PT} . The activation energies are also quite similar.

Figure 12 and figure s3 show the relative amplitude of the two rotamers of S205A and S205V respectively in both H_2O and D_2O as a function of $1/T$. At $T > 240$ K in H_2O the amplitude of the fast component is large, i.e., $a \geq 0.77$. At 295 K it is 0.96, and as the temperature decreases, it also decreases. Below 170 K the amplitudes of both time components are equal, i.e., ~ 0.5 and temperature independent. The low temperature result is in accord with the X-ray structure analysis, which suggests that at 100 K the population sizes of both rotamers are equal. In D_2O the relative amplitudes of the fast and slow decay components are about the same. At high temperatures both amplitudes strongly fluctuate around the average value of 0.5. At low temperatures, the amplitude of the fast decaying component in both H_2O and D_2O is 0.5, which indicates that Rot2 exists at these temperatures. The time-resolved emission data of the ROH^* and RO^{-*} forms of the chromophore unequivocally show that PT occurs at low temperatures in both H_2O and D_2O . It is shown in figure 11 that k_{PT} is temperature independent at sufficiently low temperatures.

The temperature dependence of k_{PT} is rather complex. At high temperatures it is strong, whereas at low temperatures there is no traceable temperature dependence though tunneling may still occur. At long hydrogen bond we expect a very large barrier and that tunneling prevails at low temperature.

The larger activation energy can be explained by the tunneling integral, as explained by the Goldanskii–Fleurov–Trakhtenberg theory¹⁸ given succinctly in the SI. Equations s2 and s3 provide a qualitative answer to the large change in the activation energy. The tunneling integral $J(R)$ (eq. s3) strongly depends on the H/D mass ratio, the potential energy, $U(R)$, and the particle's energy, $E(R)$ (zero-point energy). The temperature dependence of the proton transfer rate constant is given in the second term of equation s3.

The temperature dependence at relatively high temperatures is partially due to the $\partial J / \partial R$ factor, which strongly depends on R at low tunneling probabilities, as is the case for both S205A and S205V. The alternative proton wire is made of a water molecule and the oxygen atom in the Thr203 residue. The distance between the oxygen atoms of the water molecule and the

Thr203 residue is \sim 3.2 Å, a considerably longer distance than in the proton wire in wt-GFP (e.g., 2.7 Å). This longer distance in the mutant leads to a large difference in the tunneling rates and also in the activation energies upon H/D exchange.

■ ASSOCIATED CONTENT

5 Supporting Information. Analysis of steady state spectra of S205A mutant in H₂O, crystallographic statistics, data and data analysis of the temperature dependence of the time-resolved emission of the S205V mutant, model of the temperature dependence of the proton transfer rate in GFP S205A mutant, and a proton tunneling model. This material is available free of charge via the Internet at <http://pubs.acs.org>.

■ AUTHOR INFORMATION

Corresponding Author

*E-mail: huppert@tulip.tau.ac.il. Phone: 972-3-6407012. Fax: 972-3-6407491.

■ ACKNOWLEDGMENT

D.H. thanks James-Franck German-Israeli Program in Laser-Matter Interaction for the grant that partially supported this work. S.J.R. acknowledges support from the National Science Foundation, MCB 208731.

■ REFERENCES

- (1) Shu, X.; Leiderman, P.; Gepshtein, R.; Smith, N. R.; Kallio, K.; Huppert, D.; Remington, S. J. *J. Protein Sci.* **2007**, *16*, 2703–2710.
- (2) Zimmer, M. *Chem. Rev.* **2002**, *102*, 759–781.
- (3) Tsien, R. Y. *Annu. Rev. Biochem.* **1998**, *67*, 509–544.
- (4) Seward, H. E.; Bagshaw, C. R. *Chem. Soc. Rev.* **2009**, *38*, 2842–2851.
- (5) Kennis, J. T. M.; Larsen, D. S.; van Stokkum, I. H. M.; Vengris, M.; van Thor, J. J.; van Grondelle, R. *Proc. Natl. Acad. Sci. U.S.A.* **2004**, *101*, 17988–17993.
- (6) van Thor, J. J.; Zanetti, G.; Ronayne, K. L.; Towrie, M. *J. Phys. Chem. B* **2005**, *109*, 16099–16108.
- (7) Chattoraj, M.; King, B. A.; Bublitz, G. U.; Boxer, S. G. *Proc. Natl. Acad. Sci. U.S.A.* **1996**, *93*, 8362–8367.
- (8) Brejc, K.; Sixma, T. K.; Kitts, P. A.; Kain, S. R.; Tsien, R. Y.; Ormo, M.; Remington, S. J. *Proc. Natl. Acad. Sci. USA* **1997**, *94*, 2306–2311.
- (9) Palm, G. J.; Zdanov, A.; Gaitanaris, G. A.; Stauber, R.; Pavlakis, G. N.; Wlodawer, A. *Nat. Struct. Biol.* **1997**, *4*, 361–365.
- (10) Stoner-Ma, D.; Jaye, A. A.; Matousek, P.; Towrie, M.; Meech, S. R.; Tongue, P. J. *J. Am. Chem. Soc.* **2005**, *127*, 2864–2865.
- (11) Lang, P. T.; Ng, H. L.; Fraser, J. S.; Corn, J. E.; Echols, N.; Sales, M.; Holton, J. M.; Alber, T. *Protein Sci.* **2010**, *19*, 1420–1431.
- (12) Lovell, S. C.; Word, J. M.; Richardson, J. S.; Richardson, D. C. *Proteins* **2000**, *40*, 389–408.
- (13) Cruickshank, D. W. J. *Acta Crystallogr.* **1960**, *13*, 774–777.
- (14) Fang, C.; Frontiera, R. R.; Tran, R.; Mathies, R. A. *Nature* **2009**, *462*, 200–204.
- (15) Millet, O.; Mittermaier, A.; Baker, D.; Kay, L. E. *J. Mol. Biol.* **2003**, *329*, 551–563.
- (16) Leiderman, P.; Huppert, D.; Agmon, N. *Biophys. J.* **2006**, *90*, 1009–1018.
- (17) Leiderman, P.; Gepshtein, R.; Tsimberov, I.; Huppert, D. *J. Phys. Chem. B* **2008**, *112*, 1232–1239.
- (18) Goldanskii, V. I.; Trakhtenberg, L. I.; Fleurov, V. N. *Tunneling Phenomena in Chemical Physics*; Gordon and Breach: New York, 1989; Chapter IV.